**Atmospheric
Chemistry
and Physics
Discussions**

Geographic and seasonal distributions of CO transport pathways and their roles in determining CO centers in the upper troposphere

L. Huang[1], R. Fu[1], J. H. Jiang[2], J. S. Wright[1], and M. Luo[2]

[1]Jackson School of Geosciences, The University of Texas at Austin, Austin, TX, USA
[2]Jet Propulsion Laboratory, California Institute of Technology, Pasadena, CA, USA

Correspondence to: L. Huang (leih@utexas.edu)

ACPD

11, 32423–32453, 2011

Geographic and seasonal distributions of CO transport

L. Huang et al.

Title Page

Abstract	Introduction
Conclusions	References
Tables	Figures

| ◄◄ | ►► |
| ◄ | ► |

Back | Close

Full Screen / Esc

Printer-friendly Version

Interactive Discussion

Abstract

Past studies have identified various pathways along which carbon monoxide (CO) in the tropical upper troposphere (UT) may have been transported from the surface. However, the roles that these transport pathways play in determining the locations and seasonality of CO in the tropical UT remain unclear. In particular, UT CO peaks during the spring and fall seasons when surface CO emission and deep atmospheric convection are moderate relative to those observed during winter and summer. We have developed a method to automate the identification of three pathways that transport CO to the UT, which makes joint use of several A-Train satellite measurements. We use this method to show that the locations and seasonality of the major UT CO centers in the tropics during 2007 were largely determined by local convective transport. On average, the "local convection" pathway, in which convection occurred within a fire region, transported significantly more CO to the UT than the "LT advection → convection" pathway, in which CO was advected within the lower troposphere from a fire region to a convective region prior to convection. To leading order, the seasonality of CO concentrations in the tropical UT followed the seasonality of the "local convection" transport pathway. The centers of highest CO peaked over Central Africa during boreal spring and over South America during austral spring, when the "local convection" transport pathway was most prevalent. During boreal winter and summer, surface CO emission and convection were located in opposite hemispheres, limiting the effectiveness of transport to the UT. In these seasons, CO was mainly transported to the UT via the "LT advection → convection" pathway, in which CO was advected within the lower troposphere from fire source regions in the winter hemisphere to convective regions in the summer hemisphere, or via the "UT advection" pathway, in which UT CO was redistributed from the summer hemisphere to the winter hemisphere.

1   Introduction

Biomass burning and fossil fuel combustion have long been recognized as globally important sources of trace gases and aerosols, especially in the tropics. Carbon monoxide (CO) plays a particularly influential role in global atmospheric chemistry. CO is a byproduct of the incomplete combustion of carbon-based fuels, and can also be produced by the oxidation of methane and non-methane hydrocarbons (Jacob, 1999). CO is an ozone (O_3) precursor (Daniel and Solomon, 1998) and serves as the primary sink of the hydroxyl radical (OH) (Thompson, 1992). The lifetime of CO in the tropical troposphere is 1–2 months, which makes it a useful tracer for studying the mass transport of air originating in regions of biomass burning or fossil fuel combustion (Edwards et al., 2006).

CO transport has been studied extensively using data from field campaigns, satellites, and numerical modeling simulations. Thompson et al. (1996), Pickering et al. (1996), and Andreae et al. (2004) have shown that local deep convection over fire regions can transport large amounts of CO from the surface to the upper troposphere (UT). This "local convection" pathway is especially strong when the convection occurs in the form of pyrocumulonimbus clouds. CO may also be transported from a fire region to a convective region within the lower troposphere (LT) and then transported to the UT by deep convection (Folkins et al., 1997; Andreae et al., 2001). This "LT advection → convection" pathway is consistent with observations that UT CO centers are often located above convective regions rather than fire regions. This pathway may be particularly relevant because fires typically occur during dry seasons when local deep convection is infrequent. CO increases in the UT may also result from advection of CO within the UT, unassociated with local convection (e.g., Ray et al., 2004). This "UT advection" pathway could promote high CO concentrations in regions of strong UT convergence. The existence and local importance of each of these three transport pathways has been clearly demonstrated by previous case studies; however, the roles and relative influences of these pathways in determining the geographic and seasonal

distributions of CO in the tropical UT have not yet been comprehensively evaluated.

Schoeberl et al. (2006) used satellite observations to describe a semi-annual cycle of CO in the UT and lower stratosphere with peaks in boreal spring (March–May) and fall (September–November). They suggested that these seasonal peaks of CO
5 were related to seasonal peaks in biomass burning in Asia, Africa, and South America. Liu et al. (2007) compared the geographic and seasonal distributions of tropical deep convection with those of CO and water vapor in the UT, and suggested that the elevated concentrations of CO in the UT observed during boreal spring and fall may have been caused by the spatiotemporal coincidence of biomass burning emissions and
10 deep convective activity over Africa and South America during these seasons. Peak CO concentrations in the UT over South America lag the peak in fire emissions by 1–2 months, suggesting that prevailing subsidence during the peak fire season (July–August) may trap CO near the surface until convection moves into the fire region during September and October (Liu et al., 2010). These studies suggest that spatial overlap
15 between surface emission and deep convective activity enhances CO transport from the surface to the UT.

Relationships between the seasonal cycle of CO concentration in the UT and the seasonal cycles of surface emission and convection are not straightforward. Emissions of CO at the surface peak during boreal fall and winter, and convective activity
20 over the tropical land area between 30° S and 30° N peaks during boreal summer and winter (Fig. 1). Mean CO concentration in the UT peaks during boreal fall, when convective activity is at a minimum. Furthermore, the mean concentration of CO in the UT is higher during boreal spring than during summer, even though surface CO emission and convective activity are both higher during summer than during spring. The lack of
25 correlations among peaks in mean CO concentration in the tropical UT and peaks in surface emission and convective activity highlights the potential importance of transport pathways. To our knowledge, the influences of seasonality in the distribution of transport pathways on the seasonality of CO concentration in the tropical UT have not yet been clearly identified or addressed.

Geographic and seasonal distributions of CO transport

L. Huang et al.

Title Page

Abstract	Introduction
Conclusions	References
Tables	Figures

◄ | ►|

◄ | ►

Back | Close

Full Screen / Esc

Printer-friendly Version

Interactive Discussion

This study aims to clarify these influences. Multiple A-Train satellite datasets are used to determine the relative importance of each transport pathway to centers of elevated CO in the tropical UT and their seasonal variations. Previous studies have used data from A-Train (L'Ecuyer and Jiang, 2010) satellites to study CO transport (e.g., Fu et al., 2006; Park et al., 2007; Barret et al., 2008; Halland et al., 2009; Jin et al., 2011). Here, we build upon these previous studies by presenting and applying an automated detection mechanism for the three different CO transport pathways described above. This method streamlines the identification of CO transport pathways by intelligently combining observations of CO in the UT from the Aura Microwave Limb Sounder (MLS), observations of convective clouds from the CloudSat radar, and observations of CO emission derived from Moderate-resolution Imaging Spectroradiometer (MODIS) fire data, as described in Sects. 2 and 3. We apply the method to quantify the relative frequency of occurrence of each transport pathway with respect to the major centers of elevated CO in the tropical UT, as presented in Sect. 4. We are then able to determine which transport pathways are primarily responsible for the major centers of elevated UT CO in the global tropics, and to reconcile the apparent mismatch between the seasonal cycle of UT CO and the seasonal cycles of surface CO emissions and convective activity, as shown in Sect. 5. The main conclusions of this work are summarized and discussed in Sect. 6.

2 Datasets

The seasonal distributions of CO concentration are described according to satellite observations taken by the Aura MLS for the upper troposphere and the Aura Tropospheric Emission Spectrometer (TES) for the lower troposphere. The location and relative strength of convective activity is estimated using satellite observations of cloud water content (CWC) taken by the CloudSat millimeter-wavelength cloud radar.

The Aura MLS detects CO in the UT and lower stratosphere region by measuring emission at 240 GHz. The vertical resolution of the CO retrieval is approximately 4

km, and the horizontal resolution is approximately 7 km across-track and 300–400 km along-track. We use Level 2 (orbital) CO derived according to the MLS Version 2.2 retrieval algorithm. Version 2.2 CO has a high bias of approximately 100 % at 215 hPa (Livesey et al., 2008); we scale the measured CO concentrations at 215 hPa by 0.5

5 to compensate for this bias. The footprint of each TES nadir observation is 5×8 km (Beer, 2006). The TES retrieval of CO profiles in the tropics is primarily sensitive to CO concentrations between 700 hPa and 200 hPa, with a retrieval uncertainty of about 10–20 % (Luo et al., 2007a, 2007b). TES cannot reliably retrieve CO in the presence of clouds.

10 CloudSat measures vertical profiles of cloud ice water content (IWC) and liquid water content (LWC) in the troposphere (Stephens et al., 2002). During 2007, the A-Train orbital configuration ensured that CloudSat observed a given location less than 6 min prior to MLS and less than 14 min prior to TES. CWC represents the sum of IWC and LWC. Measurements of CWC are provided at a vertical resolution of approximately

15 500 m (Stephens et al., 2002), with a horizontal resolution of 1.7 km along-track by 1.3 km across-track.

CO emission at the surface is obtained from the Global Fire Emission Database version 2.1 (GFED v2.1) (van der Werf et al., 2006; Randerson et al., 2007). This data is provided at $1° \times 1°$ gridded horizontal resolution for the period January 1997–

20 December 2007, and comprises burned area, fuel loads, combustion completeness, and fire emissions. Emissions of fire generated trace gases (e.g., CO, CH_4, and NO_x) are derived by combining information on burned area with MODIS fire hot spots (Giglio et al., 2006), biogeochemical model estimates of fuel burned, and emission factors for each species. We used fire emissions from the GFED v2.1 re-sampled to monthly

25 intervals using MODIS fire counts for the seasonal distributions, and re-sampled to 8-day intervals for pathway identification (Giglio et al., 2003).

The horizontal resolutions of MLS, TES, and CloudSat observations are homogenized by averaging the MLS, TES, and CloudSat data over $4°$ latitude $\times 8°$ longitude grid boxes. The observations are further averaged over 8-day periods to match the

temporal resolution of the CO emission data.

We use three-dimensional wind velocities from the National Centers for Environmental Prediction/National Center for Atmospheric Research (NCEP/NCAR) reanalysis (Kalnay et al., 1996) at 12 pressure levels between 1000 and 100 hPa for illustrative purposes. The daily wind data cover the same period as the MLS observations, and are averaged over the same 8-day period at the reanalysis horizontal resolution of $2.5° \times 2.5°$.

3 Methodology

CO has a relatively long life-time in the UT. Accordingly, we diagnose the influence of transport fluxes on UT CO concentration by evaluating the change in mean CO concentrations at 215 hPa between two consecutive 8-day periods. Vertically integrated CloudSat CWC above 6 km is used to represent the strength of deep convective activity during the 8-day period.

We automate the identification of different pathways that transport CO to the UT according to the following judgment criteria, which are based on observed distributions of surface emission from the GFED database, deep convective activity from CloudSat, and changes in UT CO concentration from MLS. The "local convection" pathway is identified when an increase of CO in the UT is detected and simultaneously co-located with surface CO emission and deep convection during an 8-day period. The "LT advection → convection" pathway is identified when an increase of CO in the UT and deep convection are simultaneously detected without co-located surface CO emission during an 8-day period. The "UT advection" pathway is identified when an increase of CO in the UT is detected in the absence of co-located deep convection during an 8-day period. The effectiveness of this method for identifying CO transport pathways is demonstrated by the following two case studies.

3.1 A boreal winter case

Figure 2 shows the spatial distributions of CO surface emission, convection, and CO concentration in the UT (215 hPa) during the 8-day period of 9–16 January 2007. The strongest CO emission was located over Northern Africa (Fig. 2a). Deep convective activity was most pronounced over Central Africa south of the equator, South America, and Indonesia, away from the strongest fire regions. The center of elevated CO in the UT over Central Africa was co-located with convective activity, southward of the primary CO emission region in Africa (Fig. 2b). The center of elevated CO in the UT over the Indian Ocean and southern tip of the Indian subcontinent was also co-located with convection southwestward of the strongest emission region. The displacements of high CO centers in the UT relative to surface source regions and the co-location of these centers with convective activity suggest that CO was advected southward within the LT to the convective regions, then transported by deep convection to the UT.

To illustrate how CO transport pathways affect the UT CO center over Southern Africa, we choose a vertical cross section from 30° S to 30° N centered on 20° E (Fig. 2c). This cross section is 8° wide in longitude, covering 16–24° E. The change in CO concentration is calculated as the difference between the 9–16 January mean and the 1–8 January mean. Strong CO emission extended from 5° S to nearly 15° N, while deep convection was located in the Southern Hemisphere between 15° S and the equator. CO increased in the UT at latitudes between 20° S and 15° N, with southerly meridional wind prevailing in the UT between 5° S and 20° N. The center of increased UT CO was co-located with deep convection, away from the emission region in the opposite hemisphere. This suggests that CO was advected in the LT from the emission region to the deep convection region, lifted to the UT, and advected northward. Thus, over Central Africa, CO appears to have been transported to the UT via the "LT advection → convection" and "local convection" pathways. The distinction between these two pathways is dependent upon the distribution of surface CO emission. Over Northern Africa, CO appears to have been transported via the "UT advection" pathway.

Title Page

Abstract | Introduction

Conclusions | References

Tables | Figures

|◄ | ►|

◄ | ►

Back | Close

Full Screen / Esc

Printer-friendly Version

Interactive Discussion

Our automated detection method appears to capture these pathways: between 16° S and 8° S, the increase of CO at 215 hPa was identified as "LT advection → convection"; between 8° S and the equator, the increase of CO at 215 hPa was identified as "local convection"; southward of 16° S and northward of the equator, the increase of CO at 215 hPa was identified as "UT advection".

To further validate these results, we integrated a seven-member back trajectory ensemble from each 215 hPa MLS observation in this region during 9–16 January 2007. Trajectories were calculated using a modified version of the Goddard Fast Trajectory model (Schoeberl and Sparling, 1995; Wright et al., 2011), driven by winds and heating rates from NASA's Global Modeling and Assimilation Office (GMAO) Modern-Era Retrospective Analysis for Research and Applications (MERRA) reanalysis (Rienecker et al., 2011). The initial isentropic positions of the trajectories were calculated using the corresponding Aura MLS observations of temperature at 215 hPa. Trajectories were initialized at the MLS observation (1 trajectory per ensemble), at ±0.5° in latitude and longitude (4 trajectories per ensemble), and at ±2 K in potential temperature (2 trajectories per ensemble), and were integrated backward in time for 8 days or until a convective source was identified.

The results of the trajectory simulations are in good agreement with the results of the automated detection mechanism (Table 1). The CO transport pathway identified by the automated method matches the pathway followed by the majority of trajectories in nine out of eleven cases, with two locations of mild disagreement. The automated method identifies "UT advection" for the 16–20° S bin whereas the trajectory analysis identifies "LT advection → convection", and the automated method identifies "local convection" for the 0–4° S bin whereas the trajectory analysis identifies "UT advection". In both of these cases, a large minority of the trajectories agrees with the automated diagnosis (41 and 44 %, respectively), indicating that they represent situational ambiguity rather than failures of the automated method. These mismatches do highlight the shortcomings of the automated method, however. In particular, the method makes concrete, binary judgments based on the presence or absence of convection and the presence

Full Screen / Esc

Printer-friendly Version

Interactive Discussion

or absence of CO emission. As a result, it does not provide information on the complexity of the distribution of CO transport pathways within each grid box. Convection is strongly variable in space and time, and the method may sometimes identify a prominent CO transport pathway rather than the dominant one. On the other hand, the automated method is much less computationally expensive, and the impacts of these shortcomings on the bulk statistics are likely to be minor. Misidentification due to the use of spatial and time mean quantities is unlikely to occur except in borderline cases, for which either identification is reasonable. The distribution of CO transport pathways at finer time and space scales is beyond the scope of this work.

3.2   A boreal spring case

30 March–6 April 2007 is chosen for the second case study because the distributions of CO emission, convection and UT CO centers during this 8-day period strongly resemble the seasonal means for boreal spring. CO emission during this period was strongest in Southeast Asia, and was relatively weak in Central Africa, Central America, and South America (Fig. 3a); however, the largest concentrations of UT CO were located over Central Africa and the Gulf of Guinea (Fig. 3b). This center of elevated UT CO concentration was largely co-located with both surface CO emission and deep convective activity. CO was low in the UT over Southeast Asia despite strong surface emission, likely due to the absence of strong co-located convective activity. As in the first case study (Sect. 3.1), we explore a cross section along $20° E$ (Fig. 3c). CO emission along this cross-section extended from $10° S$ to $15° N$ and overlapped with deep convection between $10° S$ and $5° N$. Increases of CO throughout the troposphere were co-located with deep convection, rising motion, and surface emission over Central Africa, suggesting that CO was transported from surface sources to the UT by the "local convection" pathway. Our automated method also diagnosed "local convection" as the dominant CO transport pathway between $8° S$ and $8° N$.

These two case studies show that the three different CO transport pathways can be successfully diagnosed through the joint use of Aura, CloudSat, and MODIS

measurements at synoptic scales. Our detection criteria capture the relationships between CO surface emission, convective activity, and the distribution of CO in the UT that are associated with these transport pathways. We now apply this method to identify geographic and seasonal variations in the relative frequencies of occurrence of differ-
5 ent CO transport pathways over Central Africa and South America between December 2006 and November 2007.

4 Seasonal Distribution of CO Transport Pathways

Figures 4–7 show the seasonal mean geographic distributions of CO emission, convective activity, and CO in the LT (681 hPa) and UT (215 hPa) during the period December
10 2006–November 2007. The occurrence frequencies of different CO transport pathways are computed for two centers of elevated UT CO in the tropics: South America (24° S–12° N, 88–32° W) and Central Africa (20° S–20° N, 16° W–40° E). The boundaries of these focus regions are denoted by red boxes in each figure.

The boreal winter seasonal mean spatial patterns of CO surface emission, convec-
15 tive activity, and CO concentration in the LT and UT over Africa and South America (Fig. 4) are similar to those of the boreal winter case study (Fig. 2). In particular, the primary fire regions and the centers of high UT CO were located in opposite hemispheres.

The topmost panels of Fig. 4 show the spatial distributions of transport pathways
20 in the South America (left) and Central Africa (right) domains. Burning was strongest between the equator and 10° N in Africa; however, due to the lack of convective activity, CO concentration increases in the UT over Northern Africa (4–20° N) were primarily attributable to the "UT advection" pathway. The "local convection" pathway was dominant over the continent in the equatorial region (8° S–4° N), while the "LT advec-
25 tion → convection" pathway was dominant in Southern Tropical Africa (8–20° S). These results suggest that CO from the primary burning regions north of the equator experienced southward cross-equatorial advection to the convective region, transport

to the UT by deep convection, and eastward and northward advection within the UT. Over South America, the highest seasonal mean concentrations of UT CO occurred to the southeast of surface emission region, over the Amazon. The "LT advection → convection" occurred over a large area within the South America analysis domain, while the "local convection" pathway was mainly confined to the northwestern and southeastern corners. These results suggest that "LT advection → convection" was the dominant pathway for transporting CO to the UT over South America between December 2006 and February 2007.

During boreal spring (Fig. 5), the largest CO concentrations in the UT were located over the Gulf of Guinea and Central Africa. This center of high UT CO had a greater geographic overlap with both high CO in the LT and areas of strong convection relative to that observed during the winter season (Fig. 4). Furthermore, greater overlap between convective activity and the fire source regions during boreal spring increased the occurrence and spatial coverage of the "local convection" pathway over the tropical African continent (12° S–12° N) relative to boreal winter. The "UT advection" pathway was prevalent over Northern Tropical Africa, while the "LT advection → convection" pathway was prevalent over Southern Tropical Africa. Over South America, concentrations of CO in the UT were lower during boreal spring than during boreal winter (austral summer). This may result from reductions in the frequencies of the "local convection" and "LT advection → convection" CO transport pathways.

During boreal summer (Fig. 6), UT CO concentrations were highest over Southeast Asia, with a broad center of high CO extending from India in the west, across Southern China, to the Western Pacific Ocean in the east (Fig. 6a). CO over Southeast Asia is largely the result of fossil fuel emissions (Jiang et al., 2007), however, which are not represented in the GFED CO emission dataset. Given this limitation of the GFED data, we instead continue to focus our analysis on South America and Africa, where emissions of fire-generated CO are strongest (Fig. 6c). Most deep convective activity in these regions during boreal summer occurred over Central America and Northern Tropical Africa.

A center of high CO is apparent in the LT over the strong surface emissions in Southern Africa (Fig. 6b), but not over South America. The daytime boundary layer and aerosol plumes are generally deeper over Africa (3–4.5 km, Labonne et al., 2007) than over South America (Martin et al., 1988; Fu et al., 1999). Smoke layers in the Amazon basin have been observed to reach 3 km in fire areas (Andreae et al., 2004), but the daytime boundary layer outside of active fire areas is generally shallower than 2 km (800 hPa) during this season. TES is sensitive to CO between 700 hPa and 200 hPa. Because the boundary layer is deeper over Africa than over South America, high CO concentrations emitted over Central Africa are more likely to be detected by TES. Extensive cloudiness over South America may also play a role by reducing the TES sampling rate.

High concentrations of CO in the LT and UT over equatorial Western Africa suggest that CO originating in fires over southern Africa was transported by LT advection to West Africa, then lifted to the UT by convection associated with the African monsoon circulation. The "local convection" pathway was prevalent only in a small equatorial region over the African continent (4° S–4° N). The locations of strongest fire-generated emissions and strongest deep convective activity are in opposite hemispheres relative to boreal winter (Fig. 4). This change causes a similar reversal in the preferred hemispherical locations of the "UT advection" and "LT advection → convection" pathways. Over South America, the "local convection" pathway was confined to the northwestern corner. The lack of a strong center of high CO in the UT over South America may be due to the relative infrequency of CO transport events relative to Central Africa (290 in South America; 360 in Central Africa).

During boreal fall (Fig. 7), the strongest surface emissions occurred in South America and Southern Africa, with a somewhat weaker center of fire-generated CO in Northern Australia (Fig. 7c). Deep convective activity was centered over Northern South America, Central Africa, and Southeast Asia. The largest CO concentrations in both the LT (Fig. 7b) and UT (Fig. 7a) were located over South America, suggesting that vertical transport of CO was locally strong. Indeed, the "local convection" pathway was

Geographic and seasonal distributions of CO transport

L. Huang et al.

Title Page

Abstract	Introduction
Conclusions	References
Tables	Figures

◀ | ▶

◀ | ▶

Back | Close

Full Screen / Esc

Printer-friendly Version

Interactive Discussion

dominant over South America during this season. A secondary center of high UT CO was observed over Central Africa. The "local convection" pathway was not as prevalent over Central Africa as over South America, and "UT advection" played a more central role in this region. In contrast to South America and Central Africa, CO remained low in the LT and UT over Northern Australia despite strong surface emission. CO emissions appear to have been largely confined to the boundary layer over this region.

5 Discussion

Figures 4–7 suggest that the seasonality of tropical mean UT CO concentration (25° S–25° N) is controlled to leading order by seasonal changes in the centers of high UT CO over Central Africa and South America. Seasonal changes in the pathways that transport CO to the UT over these two regions therefore appear to play key roles in determining the seasonal cycle of UT CO in the tropics.

During our analysis period, CO emission over Central Africa peaked during boreal winter, while convective activity was nearly constant throughout the year (Fig. 8a, bottom). Meanwhile, CO concentrations in the UT peaked during boreal spring and fall (Fig. 8a, top). The seasonal variation of the occurrence frequency of the "local convection" pathway (Fig. 8a, middle) was similar to that of UT CO concentration. This result suggests that the seasonal prevalence of the "local convection" pathway plays a key role in the seasonal variation of UT CO over Central Africa. During boreal winter and summer, the primary fire regions and the convectively active regions were located in opposite hemispheres. Accordingly, the "local convection" transport pathway occurred infrequently, leading to lower concentrations of CO in the UT. CO emission over South America peaked during austral spring, while deep convection peaked during austral summer and fall (Fig. 8b, bottom). CO concentrations in the UT decreased monotonically from austral summer to winter, followed by a peak during austral spring. As with Central Africa, the seasonal variation of UT CO over South America was consistent with that of the occurrence frequency of the "local convection" pathway. The seasonality of

the UT CO over Central Africa and South America does not follow those of CO surface emission or convection. Figure 8 suggests that it primarily follows the seasonality of CO transport by the "local convection" pathway.

Figure 9 shows the annual average increase of CO concentrations at 215 hPa associated with the "local convection" and "LT advection → convection" transport pathways. The "UT advection" pathway represents the redistribution of CO within the UT rather than the introduction of new CO, so it is not considered here. Over Central Africa, the average increase of CO due to transport by "local convection" is approximately 1–5 ppbv (10–50 %) higher than that due to transport by "LT advection → convection". Over South America, the increase of UT CO associated with "local convection" is about 1.5–7.5 ppbv (12–59 %) higher than that associated with "LT advection → convection". These results suggest that the "local convection" pathway is more effective at transporting CO from surface to the UT than the "LT advection → convection" pathway. The enhancement of CO increases over South America relative to those over Central Africa may be due to higher surface emissions and a more rapid advance of convection into the primary fire regions during the transition from dry season to wet season (Horel et al., 1989, Li and Fu 2006).

6 Conclusions

We have presented a method that provides an automated identification of three pathways that transport CO to the UT. The method makes joint use of several A-Train satellite measurements, including Aura MLS CO, CloudSat CWC, and GFED CO emission data derived from MODIS fire counts. Two case studies, one for boreal winter and one for boreal spring, have demonstrated the effectiveness of our method for identifying CO transport pathways.

Seasonal maps of the UT CO distribution from December 2006 to November 2007 (Figs. 4–7) show that the primary centers of high UT CO were located over Central Africa during boreal spring and over South America during austral spring. In both of

these regions, the seasonal cycle of UT CO coincided with the seasonal cycle of the occurrence frequency of the "local convection" pathway. Convective activity and, to some extent, surface CO emissions were stronger during boreal winter and summer than during boreal spring and fall; however, CO emissions and convection were generally located in opposite hemispheres during boreal winter and summer. During these seasons, the transport of CO to the UT occurred mainly via the "LT advection → convection" pathway, in which CO was advected from its source region in the winter hemisphere to convective regions in the summer hemisphere, or via the "UT advection" pathway, in which UT CO was redistributed from the summer hemisphere to the winter hemisphere. The "local convection" pathway is significantly more effective at transporting CO to the UT than the "LT advection → convection" pathway. Accordingly, the seasonality of CO concentrations in the tropical UT follows the seasonality of the "local convection" transport pathway.

Our results also indicate geographic and seasonal variations in the dominant CO transport pathways, with strong dependences on surface climate conditions and circulation patterns. We must therefore be cautious about generalizing these results, which are based on a limited time period. In future work, we will apply the method that we developed for this study to a longer period to assess the climatological distribution of transport pathways over the tropical continents, and we will use these results to examine variability at seasonal and interannual timescales.

References

Andreae, M. O., Artaxo, P., Fischer, H., Freitas, S. R., Gregoire, J. M., Hansel, A., Hoor P., Kormann, R., Krejci, R., Lange, L., Lelieveld, J., Lindinger, W., Longo, K., Peters, W., de Reus, M., Scheeren, B., Silva-Dias, M. A. F., Strom, J., van Velthoven, P. F. J., and

Williams, J.: Transport of biomass burning smoke to the upper troposphere by deep convection in the equatorial region, Geophys. Res. Lett., 28, 951–954, doi:10.1029/2000GL012391, 2001.

Andreae, M. O., Rosenfeld, D., Artaxo, P., Costa, A. A., Frank, G. P., Longo, K. M., and Silva-Dias, M. A. F.: Smoking rain clouds over the Amazon, Science, 303, 1337–1342, 2004.

Barret, B., Ricaud, P., Mari, C., Attié, J.-L., Bousserez, N., Josse, B., Le Flochmoën, E., Livesey, N. J., Massart, S., Peuch, V.-H., Piacentini, A., Sauvage, B., Thouret, V., and Cammas, J.-P.: Transport pathways of CO in the African upper troposphere during the monsoon season: a study based upon the assimilation of spaceborne observations, Atmos. Chem. Phys., 8, 3231–3246, doi:10.5194/acp-8-3231-2008, 2008.

Beer, R.: TES on the Aura Mission: Scientific Objectives, Measurements, and Analysis Overview, IEEE T. Geosci. Remote, 44, 1102–1105, 2006.

Daniel, J. S. and Solomon, S.: On the climate forcing of carbon monoxide, J. Geophys. Res., 103(D11), 13249–13260, doi:10.1029/98JD00822, 1998.

Edwards, D. P., Emmons, L. K., Gille, J. C., Chu, A., Attie, J. L., Giglio, L., Wood, S. W., Haywood, J., Deeter, M. N., Massie, S. T., Ziskin, D. C., and Drummond, J. R.: Satellite-observed pollution from Southern Hemisphere biomass burning, J. Geophys. Res., 111, D14312, doi:10.1029/2005JD006655, 2006.

Folkins, I., Chatfield, R., Baumgardner, D., and Proffitt, M.: Biomass burning and deep convection in Southeastern Asia: Results from ASHOE/MAESA, J. Geophys. Res., 102(D11), 13291–13299, doi:10.1029/96JD03711, 1997.

Fu, R., Zhu, B., and Dickinson, R. E.: How do atmosphere and land surface influence seasonal changes of convection in the tropical Amazon?, J. Climate, 12(5), 1306–1321, 1999.

Fu, R., Hu, Y. L., Wright, J. S., Jiang, J. H., Dickinson, R. E., Chen, M. X., Filipiak, M., Read, W. G., Waters, J. W., and Wu, D. L.: Short circuit of water vapor and polluted air to the global stratosphere by convective transport over the Tibetan Plateau, P. Natl. Acad. Sci. USA, 103, 5664–5669, doi:10.1073/pnas.0601584103, 2006.

Giglio, L., Descloitres, J., Justice, C. O., and Kaufman, Y. J.: An enhanced contextual fire detection algorithm for MODIS, Remote Sens. Environ., 87, 273–282, doi:10.1016/s0034-4257(03)00184-6, 2003.

Giglio, L., van der Werf, G. R., Randerson, J. T., Collatz, G. J., and Kasibhatla, P.: Global estimation of burned area using MODIS active fire observations, Atmos. Chem. Phys., 6, 957–974, doi:10.5194/acp-6-957-2006, 2006.

Halland, J. J., Fuelberg, H. E., Pickering, K. E., and Luo, M.: Identifying convective transport of carbon monoxide by comparing remotely sensed observations from TES with cloud modeling simulations, Atmos. Chem. Phys., 9, 4279–4294, doi:10.5194/acp-9-4279-2009, 2009.

Horel, J. D., Hahmann, A. N., and Geisler, J. E.: An investigation of the annual cycle of convective activity over the tropical Americas, J. Climate, 2, 1388–1403, 1989.

Jacob, D. J.: Introduction to Atmospheric Chemistry, Princeton University Press, Princeton, New Jersey, USA, 1999.

Jiang, J. H., Livesey, N. J., Su, H., Neary, L., McConnell, J. C., and Richards, N. A. D.: Connecting surface emissions, convective uplifting, and long-range transport of carbon monoxide in the upper-troposphere: New observations from the Aura Microwave Limb Sounder, Geophys. Res. Lett. 34, L18812, doi:10.1029/2007GL030638, 2007.

Jin, J. J., Livesey, N. J., Jiang, J. H., Lupu, A., Kaminski, J. W., and McConnell, J. C.: Seasonal variation of trans-Pacific transport of carbon monoxide (CO) in the upper troposphere: MLS observations and GEOS-Chem and GEM-AQ simulations, Atmos. Chem. Phys. Discuss., 11, 3219–3250, doi:10.5194/acpd-11-3219-2011, 2011.

Kalnay, E., Kanamitsu, M., Kistler, R., Collins, W., Deaven, D., Gandin, L., Iredell, M., Saha, S., White, G., Woollen, J., Zhu, Y., Leetmaa, A., Reynolds, B., Chelliah, M., Ebisuzaki, W., Higgins, W., Janowiak, J., Mo, K. C., Ropelewski, C., Wang, J., Jenne, R., and Joseph, D.: The NCEP/NCAR 40-year reanalysis project, B. Am. Meteorol. Soc., 77, 437–472, 1996.

Labonne, M., Bréon, F.-M. and Chevallier, F.: Injection height of biomass burning aerosols as seen from a spaceborne lidar, Geophys. Res. Lett., 34, L11806, doi:10.1029/2007GL029311, 2007.

L'Ecuyer, T. S. and Jiang, J. H.: Touring the atmosphere aboard the A-Train, Phys. Today, 63 (7), 36–41, 2010.

Li, W. H. and Fu, R.: Influence of cold air intrusions on the wet season onset over Amazonia, J. Climate, 19, 257–275, doi:10.1175/JCLI3614.1, 2006.

Liu, C. T., Zipser, E., Garrett, T., Jiang, J. H., and Su, H.: How do the water vapor and carbon monoxide "tape recorders" start near the tropical tropopause? Geophys. Res. Lett., 34, L09804, doi:10.1029/2006GL029234, 2007.

Liu, J., Logan, J. A., Jones, D. B. A., Livesey, N. J., Megretskaia, I., Carouge, C., and Nedelec, P.: Analysis of CO in the tropical troposphere using Aura satellite data and the GEOS-Chem model: insights into transport characteristics of the GEOS meteorological products, Atmos. Chem. Phys., 10, 12207–12232, doi:10.5194/acp-10-12207-2010, 2010.

Title Page

Abstract | Introduction

Conclusions | References

Tables | Figures

|◄ | ►|

◄ | ►

Back | Close

Full Screen / Esc

Printer-friendly Version

Interactive Discussion

Livesey, N. J., Filipiak, M. J., Froidevaux, L., Read, W. G., Lambert, A., Santee, M. L., Jiang, J. H., Pumphrey, H. C., Waters, J. W., Cofield, R. E., Cuddy, D. T., Daffer, W. H., Drouin, B. J., Fuller, R. A., Jarnot, R. F., Jiang, Y. B., Knosp, B. W., Li, Q. B., Perun, V. S., Schwartz, M. J., Snyder, W. V., Stek, P. C., Thurstans, R. P., Wagner, P. A., Avery, M., Browell, E. V., Cammas, J. P., Christensen, L. E., Diskin, G. S., Gao, R. S., Jost, H. J., Loewenstein, M., Lopez, J. D., Nedelec, P., Osterman, G. B., Sachse, G. W., and Webster, C. R.: Validation of aura microwave limb sounder O_3 and CO observations in the upper troposphere and lower stratosphere, J. Geophys. Res., 113, D15S02, doi:10.1029/2007JD008805, 2008.

Luo, M., Rinsland, C., Fisher, B., Sachse, G., Diskin, G., Logan, J., Worden, H., Kulawik, S., Osterman, G., Eldering, A., Herman, R., and Shephard, M.: TES carbon monoxide validation with DACOM aircraft measurements during INTEX-B 2006, J. Geophys. Res., 112, D24S48, doi:10.1029/2007JD008803, 2007a.

Luo, M., Rinsland, C. P., Rodgers, C. D., Logan, J. A., Worden, H., Kulawik, S., Eldering, A., Goldman, A., Shephard, M. W., Gunson, M., and Lampel, M.: Comparison of carbon monoxide measurements by TES and MOPITT: Influence of a priori data and instrument characteristics on nadir atmospheric species retrievals, J. Geophys. Res., 112, D09303, doi:10.1029/2006JD007663, 2007b.

Martin, C. L., Fitzjarrald, D., Garstang, M., Oliveira, A. P., Greco, S., and Browell, E.: Structure and growth of the mixing layer over the amazonian rain forest, J. Geophys. Res., 93(D2), 1361–1375, doi:10.1029/JD093iD02p01361, 1988.

Park, M., Randel, W. J., Gettelman, A., Massie, S. T., and Jiang, J. H.: Transport above the Asian summer monsoon anticyclone inferred from aura microwave limb sounder tracers, J. Geophys. Res., 112, D16309, doi:10.1029/2006JD008294, 2007.

Pickering, K. E., Thompson, A. M., Wang, Y., Tao, W.-K., McNamara, D. P., Kirchhoff, V. W. J. H., Heikes, B. G., Sachse, G. W., Bradshaw, J. D., Gregory, G. L., and Blake, D. R.: Convective transport of biomass burning emissions over Brazil during TRACE A, J. Geophys. Res., 101(D19), 23993–24012, doi:10.1029/96JD00346, 1996.

Randerson, J. T., van der Werf, G. R., Giglio, L., Collatz, G. J., and Kasibhatla, P. S.: Global Fire Emissions Database, Version 2 (GFEDv2.1). Data set. available at: http://daac.ornl.gov/, last access: 30 May 2010, doi:10.3334/ORNLDAAC/849, from Oak Ridge National Laboratory Distributed Active Archive Center, Oak Ridge, Tennessee, USA, 2007.

Ray, E. A., Rosenlof, K. H., Richard, E. C., Hudson, P. K., Cziczo, D. J., Loewenstein, M., Jost, H.-J., Lopez, J., Ridley, B., Weinheimer, A., Montzka, D., Knapp, D., Wofsy, S. C.,

Title Page

Abstract | Introduction

Conclusions | References

Tables | Figures

|◄ | ►|

◄ | ►

Back | Close

Full Screen / Esc

Printer-friendly Version

Interactive Discussion

Daube, B. C., Gerbig, C., Xueref, I., and Herman, R. L.: Evidence of the effect of summertime midlatitude convection on the subtropical lower stratosphere from CRYSTAL-FACE tracer measurements, J. Geophys. Res., 109, D18304, doi:10.1029/2004JD004655, 2004.

Rienecker, M. M., Suarez, M. J., Gelaro, R., Todling, R., Bacmeister, J., Liu, E., Bosilovich, M. G., Schubert, S. D., Takacs, L., Kim, G.-K., Bloom, S., Chen, J., Collins, D., Conaty, A., da Silva, A., Gu, W., Joiner, J., Koster, R. D., Lucchesi, R., Molod, A., Owens, T., Pawson, S., Pegion, P., Redder, C. R., Reichle, R., Robertson, F. R., Ruddick, A. G., Sienkiewicz, M., and Woollen, J.: MERRA: NASA's Modern-Era Retrospective Analysis for Research and Applications, J. Climate, 24, 3624–3648, doi:10.1175/JCLI-D-11-00015.1, 2011.

Schoeberl, M. R. and Sparling, L.: Trajectory modeling, in: Diagnostic Tools in Atmospheric Physics, edited by: Fiocco, G. and Visconti, G., Proceedings of the International School of Physics "Enrico Fermi", 124, 289–306, 1995.

Schoeberl, M. R., Duncan, B. N., Douglass, A. R., Waters, J., Livesey, N., Read, W., and Filipiak, M.: The carbon monoxide tape recorder, Geophys. Res. Lett., 33, L12811, doi:10.1029/2006GL026178, 2006.

Stephens, G. L., Vane, D. G., Boain, R. J., Mace, G. G., Sassen, K., Wang, Z., Illingworth, A. J., O'Connor, E. J., Rossow, W. B., Durden, S. L., Miller, S. D., Austin, R. T., Benedetti, A., Mitrescu, C., and the CloudSat Science Team: The CLOUDSAT mission and the A-TRAIN: a new dimension of space-based observations of clouds and precipitation, B. Am. Meteorol. Soc., 83, 1771–1790, 2002.

Thompson, A. M.: The Oxidizing Capacity of the Earth's Atmosphere: Probable Past and Future Changes, Science, 256, 1157–1165, 1992.

Thompson, A. M., Pickering, K. E., McNamara, D. P., Schoeberl, M. R., Hudson, R. D., Kim, J. H., Browell, E. V., Kirchhoff, V. W. J. H., and Nganga, D.: Where did tropospheric ozone over Southern Africa and the Tropical Atlantic come from in October 1992? Insights from TOMS, GTE TRACE A, and SAFARI 1992, J. Geophys. Res., 101(D19), 24251–24278, doi:10.1029/96JD01463, 1996.

van der Werf, G. R., Randerson, J. T., Giglio, L., Collatz, G. J., Kasibhatla, P. S., and Arellano Jr., A. F.: Interannual variability in global biomass burning emissions from 1997 to 2004, Atmos. Chem. Phys., 6, 3423-3441, doi:10.5194/acp-6-3423-2006, 2006.

Wright, J. S., Fu, R., Fueglistaler, S., Liu, Y. S., and Zhang, Y.: The influence of summertime convection over Southeast Asia on water vapor in the tropical stratosphere, J. Geophys. Res., 116, D12302, doi:10.1029/2010JD015416, 2011.

Geographic and seasonal distributions of CO transport

L. Huang et al.

Table 1. Validation of our automated detection method using back trajectories for the case study described in Sect. 3.1 (9–16 January 2007 along 20° E). From left, columns indicate the grid box for which a pathway was identified, the pathway identified by the automated method, the pathway followed by the majority of trajectories, and the fraction of trajectories that agree with the automated identification.

Grid box	Identified pathway	Trajectory pathway	TrjFrac
28–24° S	UT advection	UT advection	100 %
24–20° S	UT advection	UT advection	94 %
20–16° S	UT advection	LT advection → convection	41 %
16–12° S	LT advection → convection	LT advection → convection	79 %
12–8° S	LT advection → convection	LT advection → convection	86 %
8–4° S	Local convection	Local convection	67 %
4° S–0°	Local convection	UT advection	44 %
0–4° N	UT advection	UT advection	93 %
4–8° N	UT advection	UT advection	100 %
8–12° N	UT advection	UT advection	100 %
12–16° N	UT advection	UT advection	100 %

Title Page

Abstract | Introduction

Conclusions | References

Tables | Figures

⏮ | ⏭

◀ | ▶

Back | Close

Full Screen / Esc
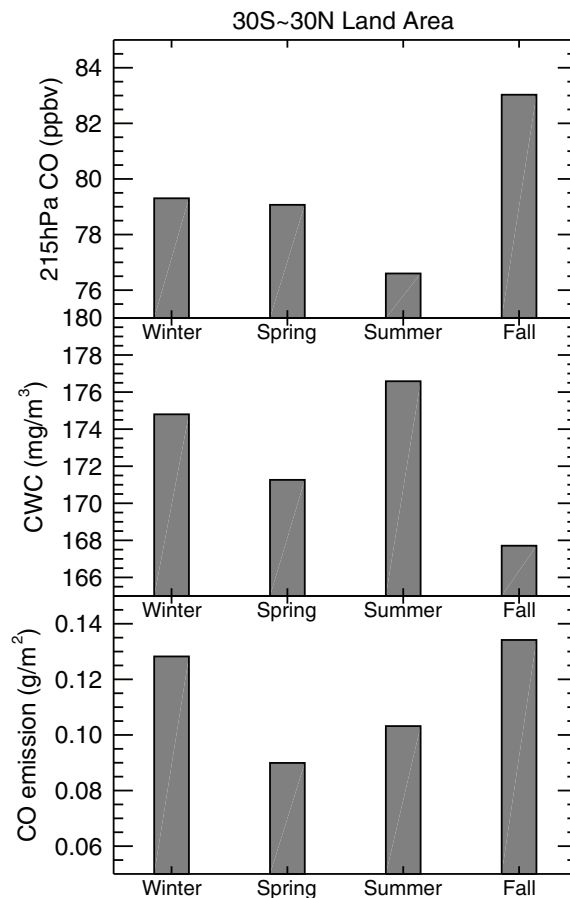
Fig. 1. Seasonal averages of MLS CO at 215 hPa (top), CloudSat cloud water content (CWC) vertically integrated above 6 km (middle), and GFED surface CO emission (bottom) over the tropical land area (30° S–30° N) during December 2006–November 2007.
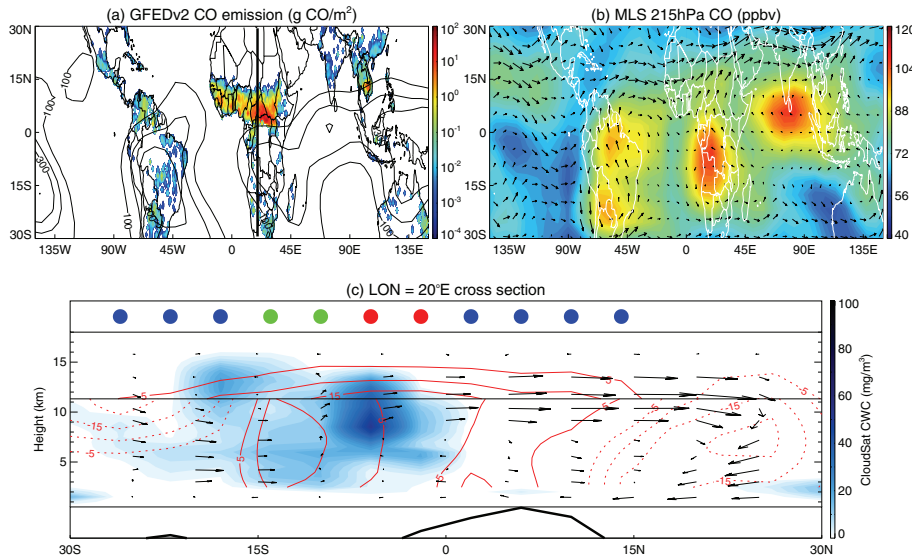
Fig. 2. (a) GFED surface CO emission (color shading) and CloudSat CWC vertically integrated above 6 km (contours). CWC contour interval is 100 mg m^{-3}. **(b)** MLS CO concentrations at 215 hPa. **(c)** Zonal mean distributions of MLS and TES CO volume mixing ratio and CloudSat cloud water content along an 8° cross-section centered at 20° E. Increases of CO are shown as red solid contours and decreases as red dashed contours, with a contour interval of 5 ppbv. NCEP/NCAR reanalysis meridional and vertical winds are shown as black arrows. The magnitude of the vertical velocity is multiplied by 100 for clarity. The thin black horizontal line at ~ 11 km indicates the boundary between MLS and TES CO. The black bold curve at the bottom indicates normalized CO emissions along the cross section. Dots along the top of panel **(c)** indicate the identified CO transport pathway: "local convection" (red), "LT advection → convection" (green), or "UT advection" (blue).
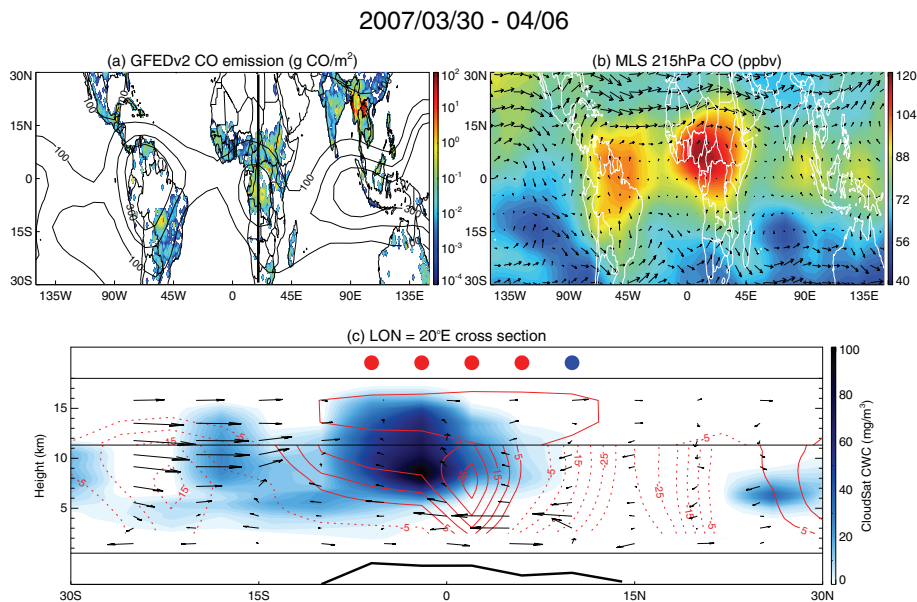
Fig. 3. As in Fig. 2, but for the period 30 March–6 April 2007.
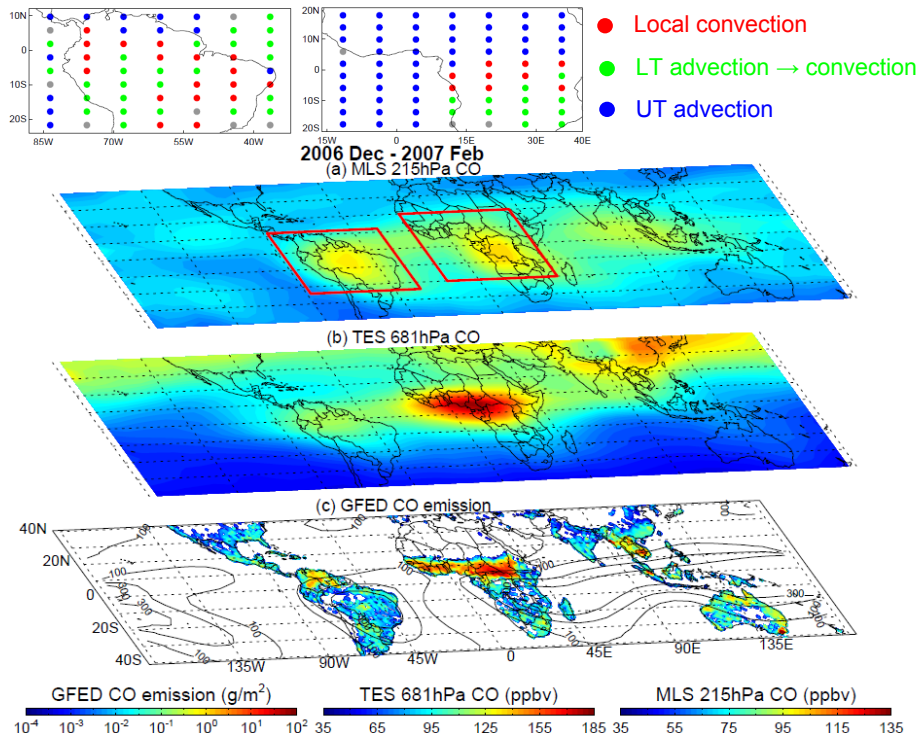
Fig. 4. Seasonal (December 2006–February 2007) mean distributions of **(a)** MLS CO in the upper troposphere (215 hPa), **(b)** TES CO in the lower troposphere (681 hPa), and **(c)** GFED surface CO emission (color shading) and CloudSat CWC vertically integrated above 6 km (contours). The CWC contour interval is $100\,\mathrm{mg\,m^{-3}}$. The two selected analysis domains are outlined in red: South America (24° S–12° N, 88–32° W) and Central Africa (20° S–20° N, 16° W–40° E). The two panels at the top show the spatial distributions of the dominant transport pathway for each $8° \times 4°$ grid box in the two analysis domains: "local convection" (red), "LT advection → convection" (green), or "UT advection" (blue). Grey dots indicate that no dominant pathway could be identified.

Title Page

Abstract | Introduction

Conclusions | References

Tables | Figures

|◄ | ►|

◄ | ►

Back | Close

Full Screen / Esc

Printer-friendly Version

Interactive Discussion

Fig. 5. As in Fig. 4, but for March–May, 2007.
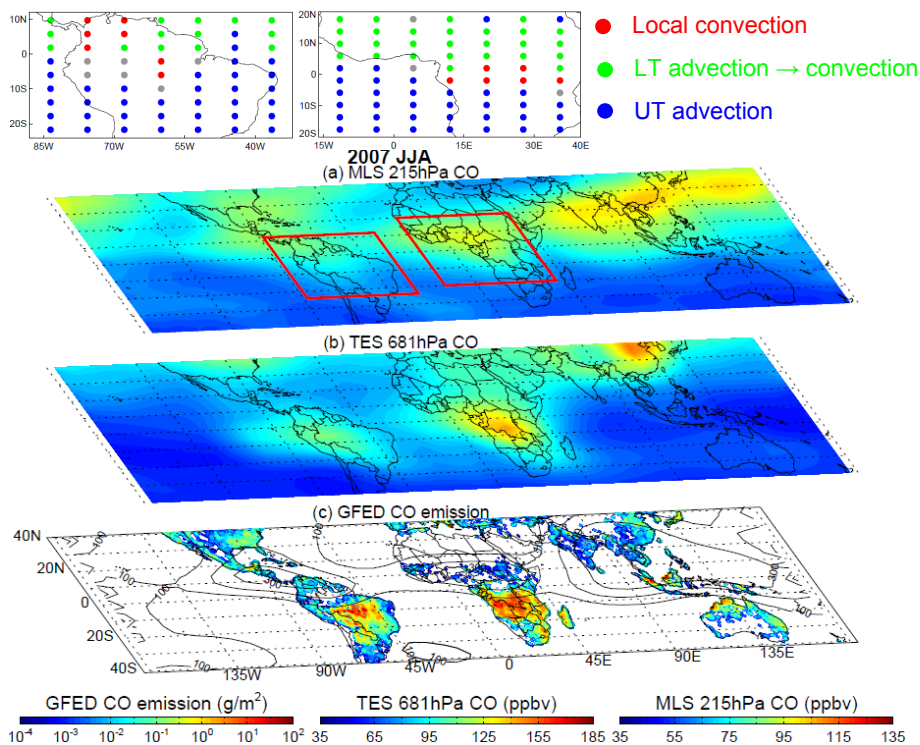
Fig. 6. As in Fig. 4, but for June–August, 2007.
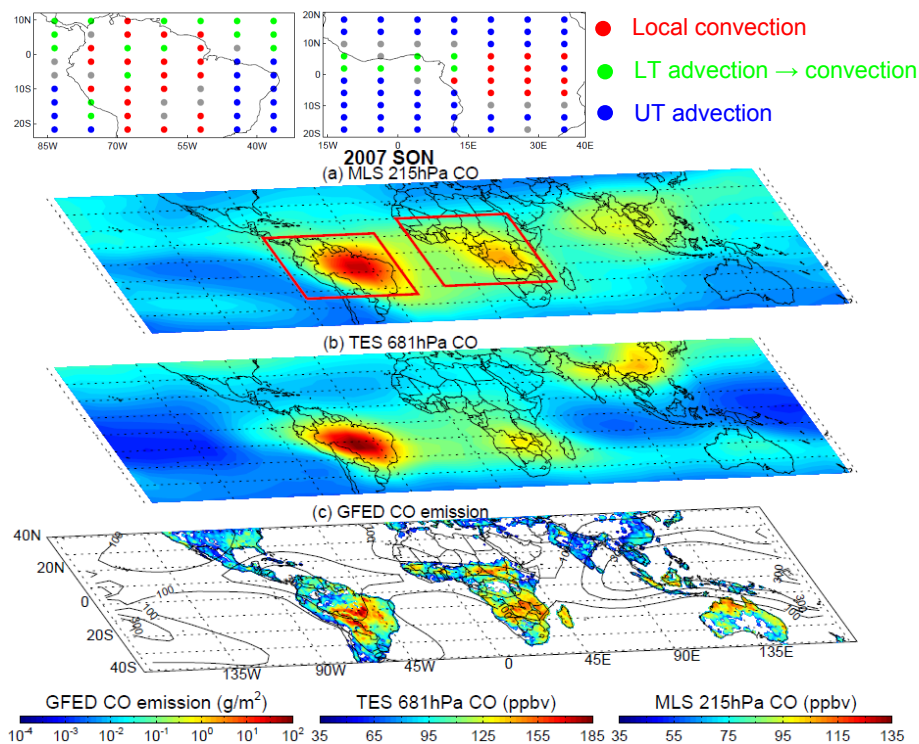
Fig. 7. As in Fig. 4, but for September–November, 2007.
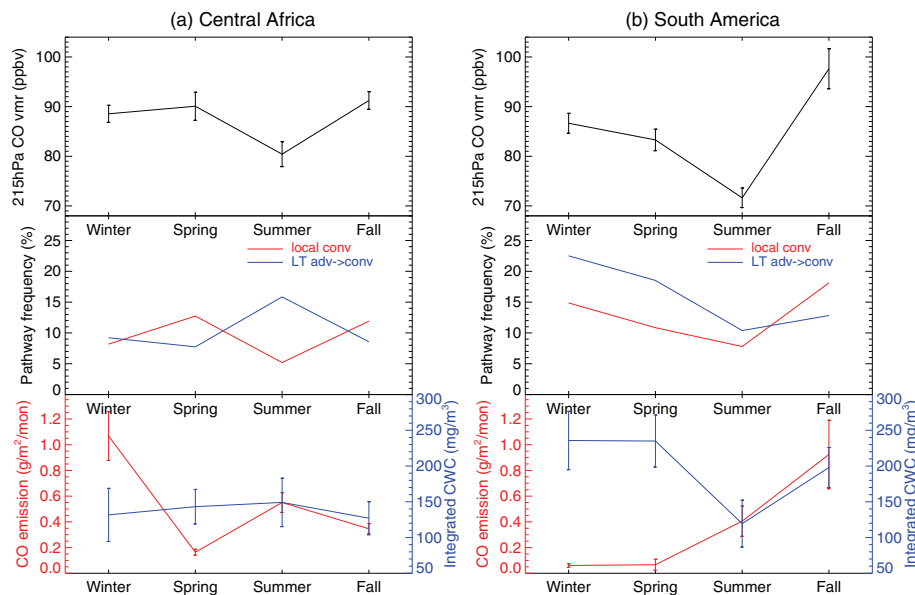
Fig. 8. Seasonal cycles of (top) MLS CO at 215 hPa, (middle) the occurrence frequencies of the "local convection" (red) and "LT advection → convection" (blue) CO transport pathways, and (bottom) GFED surface CO emission (red) and CloudSat CWC vertically integrated above 6 km (blue) for **(a)** Central Africa (20° S–20° N, 16° W–40° E) and **(b)** South America (24° S–12° N, 88–32° W) from December 2006–November 2007. Pathway frequencies represent the occurrence frequency relative to all events (both transport and non-transport) in each region. Error bars encompass ±2 standard error from the mean.
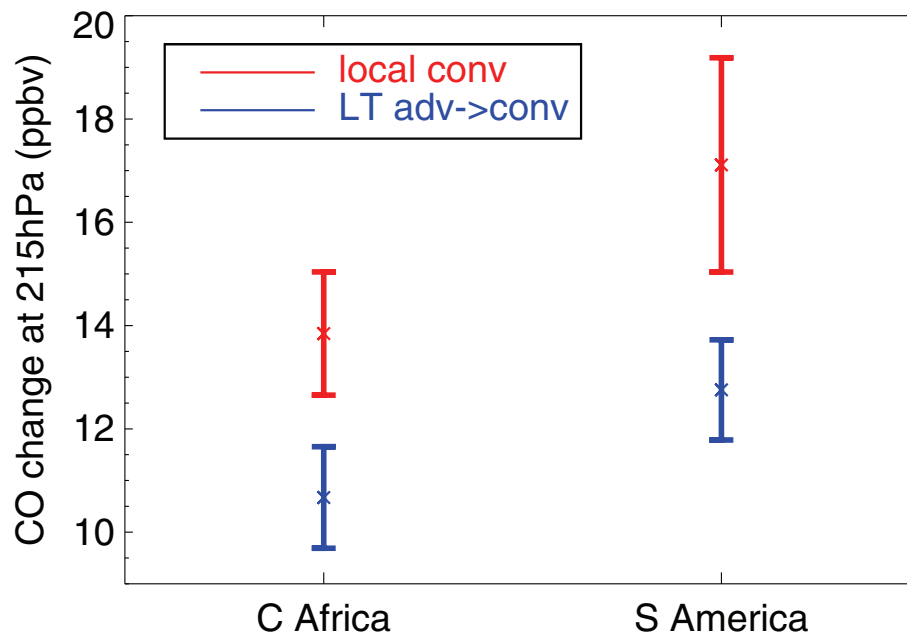
Fig. 9. Annual mean increase of CO concentrations at 215 hPa associated with the "local convection" (red) and "LT advection → convection" (blue) CO transport pathways. Error bars encompass ±2 standard error from the mean.